ACS OMEGA

Open Access

http://pubs.acs.org/journal/acsodf

Article

GASP: A Pan-Specific Predictor of Family 1 Glycosyltransferase Acceptor Specificity Enabled by a Pipeline for Substrate Feature Generation and Large-Scale Experimental Screening

David Harding-Larsen, Christian Degnbol Madsen, David Teze, Tiia Kittilä, Mads Rosander Langhorn, Hani Gharabli, Mandy Hobusch, Felipe Mejia Otalvaro, Onur Kırtel, Gonzalo Nahuel Bidart, Stanislav Mazurenko, Evelyn Travnik, and Ditte Hededam Welner*

Cite This: *ACS Omega* 2024, 9, 27278−27288

Read Online

ACCESS | Metrics & More | Article Recommendations | Supporting Information

ABSTRACT: Glycosylation represents a major chemical challenge; while it is one of the most common reactions in Nature, conventional chemistry struggles with stereochemistry, regioselectivity, and solubility issues. In contrast, family 1 glycosyltransferase (GT1) enzymes can glycosylate virtually any given nucleophilic group with perfect control over stereochemistry and regioselectivity. However, the appropriate catalyst for a given reaction needs to be identified among the tens of thousands of available sequences. Here, we present the glycosyltransferase acceptor specificity predictor (GASP) model, a data-driven approach to the identification of reactive GT1:acceptor pairs. We trained a random forest-based acceptor predictor on literature data and validated it on independent in-house generated data on 1001 GT1:acceptor pairs, obtaining an AUROC of 0.79 and a balanced accuracy of 72%. The performance was stable even in the case of completely new GT1s and acceptors not present in the training data set, highlighting the pan-specificity of GASP. Moreover, the model is capable of parsing all known GT1 sequences, as well as all chemicals, the latter through a pipeline for the generation of 153 chemical features for a given molecule taking the CID or SMILES as input (freely available at https://github.com/degnbol/GASP). To investigate the power of GASP, the model prediction probability scores were compared to GT1 substrate conversion yields from a newly published data set, with the top 50% of GASP predictions corresponding to reactions with >50% synthetic yields. The model was also tested in two comparative case studies: glycosylation of the antihelminth drug niclosamide and the plant defensive compound DIBOA. In the first study, the model achieved an 83% hit rate, outperforming a hit rate of 53% from a random selection assay. In the second case study, the hit rate of GASP was 50%, and while being lower than the hit rate of 83% using expert-selected enzymes, it provides a reasonable performance for the cases when an expert opinion is unavailable. The hierarchal importance of the generated chemical features was investigated by negative feature selection, revealing properties related to cyclization and atom hybridization status to be the most important characteristics for accurate prediction. Our study provides a GT1:acceptor predictor which can be trained on other data sets enabled by the automated feature generation pipelines. We also release the new in-house generated data set used for testing of GASP to facilitate the future development of GT1 activity predictors and their robust benchmarking.

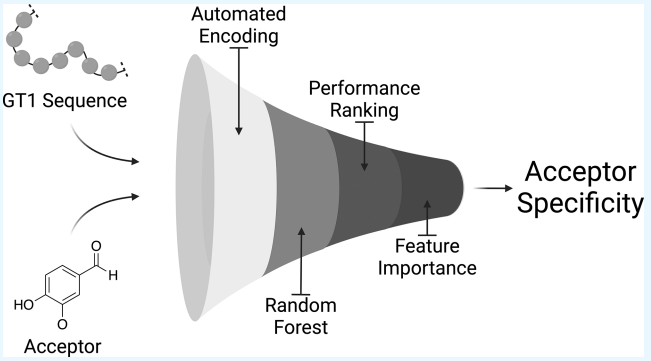

INTRODUCTION

Glycosylation is a crucial step to obtain a plethora of biologically and industrially relevant molecules, from proteins to natural products and artificial compounds.[1] Accordingly, glycosylation is one of the most common reactions in the biosphere. However, to achieve the required control of stereo- and regioselectivity, organic chemists apply a succession of reactions, including protecting group manipulations and bond activations, amounting to low chemical yields, poor atom economy, and large amounts of waste.[2,3] In Nature, these reactions are mainly catalyzed by glycosyltransferases, enzymes which offer perfect stereoselectivity and often high regioselectivity in a single reaction with unprotected substrates.[4,5] However, the factors governing acceptor specificity and regioselectivity of glycosyltransferase reactions are poorly understood, making it challenging to select an appropriate biocatalyst without extensive experimentation.[6]

Received: February 19, 2024
Revised: May 27, 2024
Accepted: May 29, 2024
Published: June 11, 2024

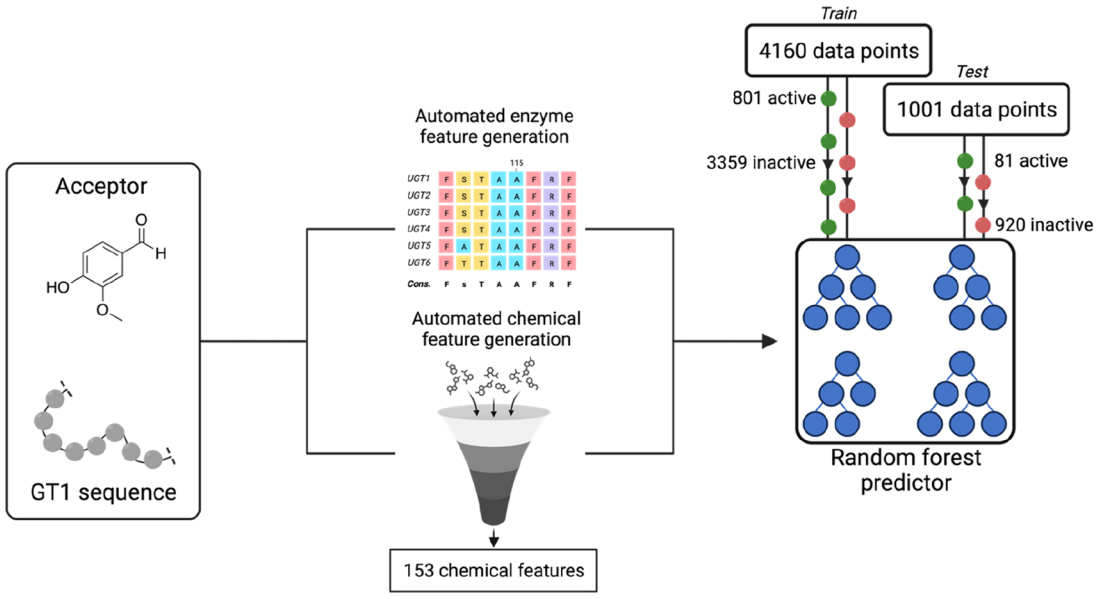

Figure 1. General concept of GASP: a GT1:acceptor pair consisting of an acceptor and a GT1 sequence is used as input to two automated feature generation pipelines: (i) the enzyme feature generation based on an MSA and BLOSUM62 encoding, with colors corresponding to amino acid type, and (ii) the substrate feature generation based on chemical features (Figure 2). These features are fed into a random forest predictor, that then returns the predicted reaction probability of the calculated GT1:acceptor pairs. GASP is trained on data from the GT-Predict publication and tested on an independent in-house data set (active pairs shown as green balls and inactive as red balls).

Glycosyltransferases are phylogenetically organized into 115 families (as of May 15th, 2023) in the Carbohydrate Active Enzymes (CAZy) database (http://www.cazy.org/).[7] Glycosylation of natural products and secondary metabolites is primarily catalyzed by glycosyltransferase family 1 (GT1) enzymes, which thus represent important biocatalysts for biotechnological applications.[1] GT1 enzymes have a GT-B fold, catalyzing glycosylation in a cleft between two Rossmann-like domains, the N-terminal domain binding mainly the acceptor substrate(s), and the C-terminal domain binding mainly the α-glycosyl donor.[8] Usually, this glycosyl donor is a uridine diphosphate-activated sugar, and thus GT1s are called UDP-dependent glycosyltransferases or UGTs.[9] They catalyze *C*-, *O*-, *N*- and *S*- glycosylation with an inversion of stereochemistry, leading to β-linked products.[10,11] The reaction proceeds through an oxocarbenium glycosyl intermediate, with the catalytic dyad sharing the abstracted proton.[12] However, while much is known about their structures and mechanisms, 59 GT1 enzymes have at least one deposited crystallographic structure and 338 are biochemically characterized as of May 15th, 2023 according to the CAZy database, little is known about their acceptor scope, except that it is tremendously varied with thousands of different acceptors being reported, and individual enzymes vary from highly specific to very promiscuous.[13,14] Their activity is difficult to infer from biological data since a single organism can contain over hundred different GT1 genes.[15]

Machine learning (ML) is emerging as a powerful tool in enzymology, due to its strength in recognizing patterns in complex data.[16,17] Accordingly, ML has previously been employed to predict enzyme−substrate specificities.[18] This includes a random forest thiolase activity predictor,[19] a gradient-boosted regression tree capable of predicting the donor specificity of GT-A fold glycosyltransferases,[20] and a random forest adenylate-forming enzyme substrate and function predictor.[21,22] In addition, a decision tree-based algorithm, GT-Predict, has been developed specifically for GT1 enzymes to predict GT1:acceptor pairs.[6] GT-Predict is trained on reactivity measurements of 54 *Arabidopsis thaliana* GT1 enzymes against 91 structurally diverse glycosylation acceptors. GT-Predict was not tested on independent data, and testing on substrates absent from the training set would require the manual addition of substrate features. For sequences outside the training data (i.e., non-*Arabidopsis* GT1 enzymes), GT-Predict returns the substrate reactivity measured experimentally for the closest *A. thaliana* homologue. Given that phylogeny has been shown to be a relatively poor predictor of GT1 specificity,[14] there is potential for further development.

In this study, we aimed to address the broad landscape of GT1:acceptor reactivity by implementing a pan-specific predictor able to process enzymes and chemicals outside the training data set. We used a random forest architecture trained on 4160 data points (each representing a GT1:acceptor pair) publicly available through the GT-Predict publication.[6] We developed an automated pipeline for enzyme and substrate feature generation, capable of parsing all known GT1 sequences and automatically generating 153 chemical features for any potential acceptor substrate, thereby allowing predictions on all GT1:acceptor pairs (Figure 1). The model, named Glycosyltransferase Acceptor Specificity Predictor (GASP), was tested on an in-house-generated independent data set of 1001 data points, demonstrating the generation of a generic predictor with a balanced accuracy of 72% to evaluate any GT1:acceptor pair. The performance of GASP was compared to baseline models, to GT-predict, to that of a group of GT1 experts for the glycosylation of the plant defensive compound 2,4-dihydroxy-1,4-benzoxazinone (DIBOA), and to random selection for the glycosylation of the essential medicine niclosamide. In addition, negative feature selection was performed to understand the importance of the 153 generated chemical features.

https://doi.org/10.1021/acsomega.4c01583
ACS Omega 2024, 9, 27278−27288

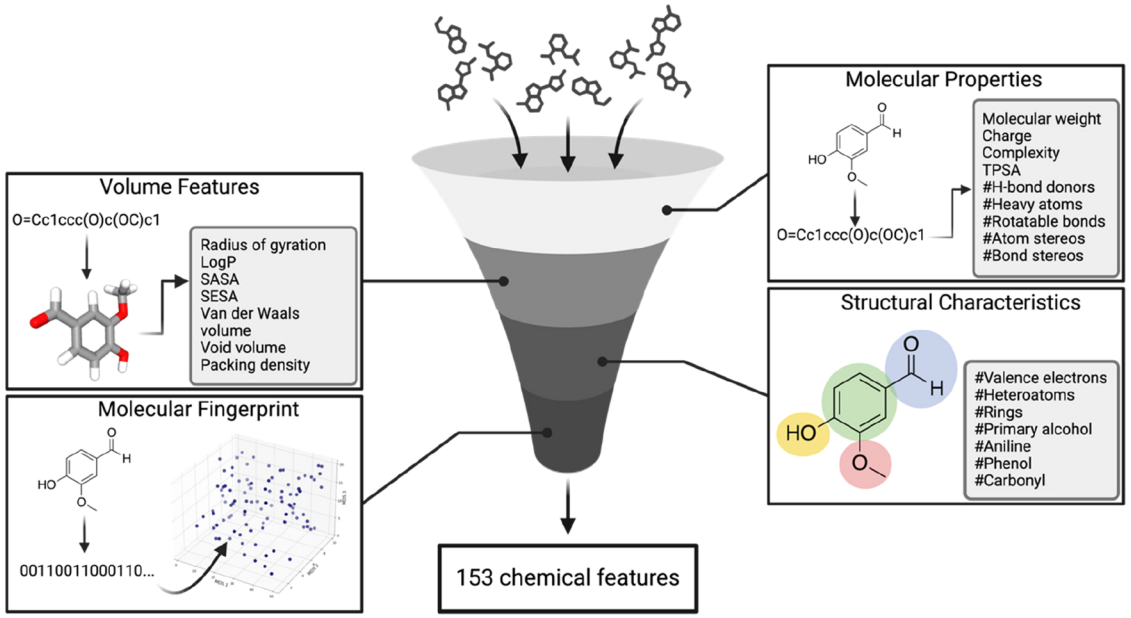

Figure 2. Chemical feature generation pipeline can take CIDs or SMILES and generate chemical features. If a CID is used, SMILES are generated from the CID. Molecular properties are then retrieved from PubChem via webchem[24] using the SMILES. The SMILES are passed to RDKit which creates a molecular representation, including 3D conformers that are written to PDBs and translated to volume features. RDKit is then used to generate structural characteristics, while E3FP[25] is used to generate molecular fingerprints from the SMILES representation (the symbol '#' indicates "number of"). All pairwise Euclidean distances are calculated between the molecular fingerprints using E3FP which are converted to projected points in a *k*-dimensional space (here, $k = 12$) using MultiDimensional Scaling (MDS). Features from all steps above are concatenated into a total of 153 chemical features.

METHODS

Test Data Set Generation. Twenty-four GT1 genes randomly selected from NCBI were synthesized by Genscript (USA) in a modified pET28a(+) vector with an N-terminal 6xHis-tag followed by a TEV-cleavage site and the gene of interest. BL21 Star (DE3) cells (ThermoFisher Scientific, USA) carrying a pET28a(+) vector with the GT1-gene of interest between restriction sites NcoI (5′) and XhoI (3′) were inoculated with 1% (v/v) overnight culture and grown at 37 °C until OD_{600} 0.5−0.8 in Luria−Bertani media supplemented with 50 μg/mL kanamycin. Protein expression was induced with 0.5 mM isopropyl-β-D-thiogalactopyranoside, and cells were grown overnight at 18 °C. Cells were harvested by centrifugation (4000*g*, 15 min, 4 °C) and stored at −20 °C. All purification steps were done on ice or in a cold room. Cell pellets were thawed and dissolved in lysis buffer (50 mM HEPES, 300 mM NaCl, 20 mM imidazole, 1 mM dithiothreitol (DTT), pH 7.4, supplemented with 1 μg/mL DNase I and one complete EDTA-free protease inhibitor cocktail (Roche) tablet per 50 mL lysis buffer). Cells were lysed via three passes through a French press (EmulsiFlex C5, Avestin), and the lysate was cleared by centrifugation (12,000*g*, 40 min, 4 °C). The supernatant was incubated with Ni-NTA beads (HisPur NiNTA resin, Thermo-Fischer) with gentle shaking (1 h), and the beads were washed three times with wash buffer (50 mM HEPES, 300 mM NaCl, 20 mM imidazole, pH 7.4). Bound proteins were eluted with elution buffer (50 mM HEPES, 300 mM NaCl, 250 mM Imidazole, pH 7.4). The buffer was exchanged to 50 mM HEPES pH 7.4, 50 mM NaCl, and 2 mM DTT for storage. The protein concentration was adjusted to 5 mg/mL (estimated by A_{280} using a Nanodrop spectrophotometer) when necessary, and aliquots were flash-frozen in liquid nitrogen and stored at −80 °C.

Each GT1 enzyme was assayed against a diverse substrate library of compounds representing a typical GT1 acceptor (n = 88, SI: Appendix) using an in-house developed NADH-coupled enzyme assay in 96-well format; UDP release by the GT1 reaction was detected by coupling it to NADH consumption through the combined action of pyruvate kinase (UDP + phosphoenolpyruvate → pyruvate) and lactate dehydrogenase (pyruvate + NADH → NAD^+ + lactate). The consumption of NADH was followed by A_{340} nm. A 150 μL of reaction mixture consisted of 3 μL of a substrate (10 mM in DMSO), 102 μL of assay buffer (50 mM HEPES, pH 7.4, 50 mM KCl, 5 mM $MgCl_2$, 1 mM EDTA, 1.5 mM DTT, 0.6 mM NADH), 15 μL of detection solution (8 mM phosphoenolpyruvate, 40 U/mL pyruvate kinase, 60 U/mL lactate dehydrogenase), and 15 μL of enzyme. The reaction was initiated by the addition of 15 μL of 10 mM UDP-α-D-glucose (UDP-Glc) and shaken linearly for 10 s before reading out A_{340} for 1 h at 15 s intervals, 25 °C, in a Synergy H1 plate reader. Data were analyzed with R (https://www.R-project.org/) using RStudio (https://www.RStudio.com). Slopes were fitted (A_{340}/sec), and initial apparent rates were calculated (k_{obs} = slope/[NADH]/[enzyme]). Background activity from enzyme preparations (no substrate added) was subtracted.

Reactivity Classification Pipeline. A pipeline was constructed for the conversion of reaction rates to reactivity Booleans (i.e., reactive and nonreactive). Reactive GT1:acceptor pairs are identified with outlier detection, since most measurements are of nonreactivity, typically with a sharp contrast to a minor set of nonzero rates (Figure S1). The outlier detection is performed independently on each enzyme by assuming the measurements follow a normal distribution $N[\mu = 0, \sigma = \sigma(\text{measurements})]$, i.e., they are all nonreactive

https://doi.org/10.1021/acsomega.4c01583
ACS Omega 2024, 9, 27278−27288

with nonzero rates occurring due to noise. From the distribution, a p-value is calculated to quantify how extreme any of the measurements are. Adjusted p-values were calculated from the p-values with the Holm method. Measurements that have both p-value > 0.05 and adjusted p-value > 0.05 are considered to fit the null hypothesis and are therefore classified as nonreactive observations, while measurements with both p-value < 0.05 and adjusted p-value < 0.05 do not fit the null-hypothesis, so are classified as observations of reactivity. Some data points have a p-value < 0.05 but adjusted p-value > 0.05 which was considered inconclusive evidence; thus, those data points were discarded.

Enzyme Feature Generation Pipeline. A pipeline was developed for generating enzyme features that incorporate GT1 enzyme sequences from experimental data sets (i.e., the test data set, GT-Predict data set, and reactions from literature) and the CAZy database (26,335 unique Genbank ID entries as of Dec. 2nd, 2021). Sequences from experimental data sets were aligned with MUSCLE[23] and combined with GT1 sequences from CAZy, filtered in length to range from 300 to 600 amino acids. Subsequently, a Hidden Markov Model was built upon the combined set of GT1 sequences using HMMER. Nonconsensus positions were discarded, where a consensus position was identified as the majority of sequences containing the same letter for that location. Sequence alignments with less than 80% identity to the consensus sequence (i.e., the sequence with the most frequent amino acids at each position) were discarded, yielding a set of 10,374 sequences. As the N-terminus region is most important for acceptor preference, each of the remaining 10,374 sequences was split in half, and only the part corresponding to the N-terminus was kept for amino acid encoding with BLOSUM62.

Substrate Feature Generation Pipeline. To enable easy prediction of an active GT1 enzyme for any acceptor substrate, we developed a pipeline for substrate feature generation: acceptors represented as PubChem CIDs are converted to SMILES and used as input to RDKit (https://www.rdkit.org), webchem,[24] and E3FP[25] to generate molecular features (Figure 2). Molecular properties are found with the RDKit software and curated from PubChem with the webchem R package.[24] In addition, RDKit is used for generating 3D representations of the chemical compounds in PDB format, which are further used to generate area and volume features with the PyMOL Molecular Graphics System (Version 2.0 Schrödinger, LLC) and ProteinVolume,[26] respectively. E3FP[25] is used for generating molecular fingerprints. The fingerprints are projected into a metric space by applying MultiDimensional Scaling (MDS) to pairwise Euclidean distances calculated between all the molecular fingerprints. Thus, the chemical features from the molecular fingerprints are represented in a 12-dimensional space. MDS was employed to reduce the dimensions of the molecular fingerprints, thereby mitigating the risk of a potential dimensionality problem. A reduction to 12 dimensions was chosen to balance the need for retaining enough information to distinguish different substrates while avoiding fingerprints dominating the substrate encoding. Furthermore, since random forest is employed, it is anticipated that any extraneous MDS features will simply be excluded from the decision trees. Ultimately, all these substrate features are concatenated to a single feature vector.

Model Training and Evaluation. GT1:acceptor pairs from the GT-Predict data set (77 chemicals and 73 GT1 enzymes, 4160 data points) was encoded using the BLOSUM62 encodings and substrate features as described previously, concatenating them both into a singular feature vector. After removing redundant features with identical values across the entire data set, the encoded GT-Predict data set was used to train and optimize a random forest predictor as follows. The effects of "n_estimators" and "max_depth" hyperparameters were first examined manually, and then a more thorough grid search of a larger set of hyperparameters was implemented based on the 5-fold cross-validation and area under the receiver operating characteristic curve AUROC (Table S1). Since an exhaustive grid search might lead to overfitting, we decided to keep both the model after manual search and the best performing model after the grid search.

The two developed models were tested using an independent in-house data set (1001 data points, see Test Data Set Generation), using the same protocol for feature generation. The AUROC, calculated with the scikit-learn metrics package[27] in Python (version 3.8.5), indicated an overfitting for the best model from the grid search (Figure S2), and consequently, the corresponding model was discarded. It should here be noted that the test set was only employed in model selection for subsequent experimental validation (see Case Study: Glycosylation of GASP-Predicted GT1s vs Expert Selection and Random Selection in Methods), and neither model was tuned toward our independent data set. The resulting model, obtained from manual parameter search, was further evaluated by the balanced accuracy, precision, recall, and F1-score. The balanced accuracy (eq 1), precision (eq 2), recall (eq 3), and F1-score (eq 4) were calculated as follows (false negative (FN), false positive (FP), true negative (TN), and true positive (TP)):

$$\text{balanced accuracy} = \frac{\frac{TP}{TP+FN} + \frac{TN}{TN+FP}}{2} \quad (1)$$

$$\text{precision} = \frac{TP}{TP+FP} \quad (2)$$

$$\text{recall} = \frac{TP}{TP+FN} \quad (3)$$

$$F_1 = 2\frac{\text{precision}\cdot\text{recall}}{\text{precision}+\text{recall}} \quad (4)$$

To calculate the confusion matrix for the reporting purposes, the threshold of 0.345 corresponding to the maximum F1-score was selected (Figure S3). However, the raw score returned by GASP was eventually used in ranking the sequences in the subsequent experimental validation (see Case Study: Glycosylation of GASP-Predicted GT1s vs Expert Selection and Random Selection).

Comparison to Baselines and Single-Task Models. To examine the performance of GASP, we constructed baseline and single-task models as described by Goldman et al.[18] (Table S2). Specifically, we trained a Levenshtein KNN model, a Tanimoto KNN model, and a Ridge Regression model trained on random features, henceforth denoted the "baseline models". Due to the limited overlap between the GT-Predict data set and the in-house data, only eight individual enzyme discovery models and six individual substrate discovery models were constructed (Table S3). In addition to these baseline models, two single-task GASP models were constructed, one for enzyme discovery and one for substrate discovery, using the

https://doi.org/10.1021/acsomega.4c01583
ACS Omega 2024, 9, 27278−27288

same overlapping enzymes and substrates as the baseline models, denoted as the "single-task models". The full GASP model was also tested on the same subset of GT1:acceptor pairs used to evaluate the enzyme and substrate discovery models. As the full GASP incorporates information about both enzyme and substrate, it is in theory able to learn the interactions between the two, known as a compound-protein interaction (CPI) model. To examine this CPI nature of GASP, we employed three different test subsets, consisting of all GT1:acceptor pairs where either the substrate, the enzyme, or both were not present in the training data set. The performance was compared to a Ridge Regression model trained on random substrate and enzyme features.

Comparison to GT-Predict. As a comparison to the performance of GT-Predict model, the leave-one-out validation protocol from the original publication was replicated using our GASP model and the *Arabidopsis thaliana* data from GT-Predict (Table S4). The performance was evaluated using accuracy (eq 5) and Matthews Correlation Coefficient (MCC) (eq 6):

$$\text{accuracy} = \frac{\text{TP} + \text{TN}}{\text{TP} + \text{FN} + \text{TN} + \text{FP}} \tag{5}$$

$$\text{MCC} = \frac{(\text{TP}\cdot\text{TN}) - (\text{FP}\cdot\text{FN})}{\sqrt{(\text{TP} + \text{FP})\cdot(\text{TP} + \text{FN})\cdot(\text{TN} + \text{FP})\cdot(\text{TN} + \text{FN})}} \tag{6}$$

All hyperparameters of the GASP leave-one-out models were the same as for the full model, as was the threshold chosen for metric calculation. It was impossible to calculate the MCC for 16 substrates due to lack of positive labels in the corresponding subset. The average MCC metric was therefore pruned of these substrates.

Comparison to Substrate Conversion Yield Data. As GASP is trained on binary activity data, it can also be used for predicting the likelihood of activity for a given GT1:acceptor pair. However, a typical data type for enzymatic assays is conversion yield, describing the percentage of the substrate being converted to the product. To examine the strength of the GASP predictions, we compared the model probability outputs with the conversion yields of the newly published GT1 data set.[28] Specifically, we examined the correlation between GASP and the conversion yield of glycosylation of polyphenols using *Gm*UGT88E3 as enzyme.[29] GASP was run for every possible *Gm*UGT88E3:acceptor pair to produce activity probabilities, with the results ranked from highest to lowest model probability.

Case Study: Glycosylation of GASP-Predicted GT1s vs Expert Selection and Random Selection. To test the performance of GASP, a small comparative case study for the glycosylation of DIBOA and niclosamide via expert-selected and GASP-predicted GT1s was carried out. Only GT1s available from our in-house library were considered. For the DIBOA case, expert-selected GT1s were inferred by employing intuition to assess the structural similarity between DIBOA and polyphenols from a publicly available data set[28] and then choosing among 40 GT1s enzymes that are known to be active on the most similar polyphenol structures, namely 5,7-dihydroxychromone, 4,7-dihydroxycoumarin, 4-methylesculetin, and 4-methyllimetol. GT1s which were active with 3 out of the 4 similar polyphenols were chosen, resulting in six protein sequences. For the selection of GASP-predicted sequences, six GT1s among the highest probability scores present in our stocks were chosen, resulting in a total number of six expert-selected versus six GASP-predicted enzymes (Table S5). GT1 enzymes BX8 (AAL57037.1) and BX9 (AAL57038.1) from *Zea mays* were chosen as positive controls.[30]

Our previous efforts for glycosylation of niclosamide had revealed that 10 out of 19 randomly selected GT1s screened were active, albeit yielding very low amounts of the niclosamide-Glc. For the case study of niclosamide, we therefore examined the performance of GASP to predict GT1s for niclosamide glycosylation. With the use of the top GASP predictions to construct an initial list of 14 sequences, 2 enzymes with SoluProt[31] scores lower than 0.450 were removed, resulting in a total number of 12 GASP-predicted GT1s.

Selected GT1s were expressed as described in the test data set generation. Proteins were extracted from 0.5−1 L cell cultures. The filtered supernatant was purified by nickel affinity chromatography (HisTrapTM FF, GE Healthcare, Sweden) on an ÄKTA pure (GE Healthcare, Sweden) system. After concentration and buffer exchange, each GT1 enzyme was assayed for glycosylation activity against DIBOA or niclosamide using UDP-Glc as the donor substrate.

The DIBOA glycosylation reactions were initiated via the addition of the 100 μg/mL enzyme to the reaction mixture of 0.5 mM DIBOA from a 50 mM stock in 100% DMSO, 2 mM UDP-Glc in water, and 100 mM citrate-phosphate buffer (pH 7.0) in a total reaction volume of 180 μL and incubated for 1 h at 30 °C while shaking linearly at 300 rpm. Thirty microliters of the reaction mixture were withdrawn and mixed with 30 μL of methanol to stop the reaction and centrifuged for 10 min to remove any precipitated proteins. Forty microliters of the resulting supernatant were then diluted to 200 μL with Milli-Q water before injection into an Ultimate 3000 Series apparatus equipped with an Agilent ZORBAX Eclipse Plus C18 column. A gradient of solutions A (0.1% aqueous formic acid) and B (100% acetonitrile) was used as mobile phase for analyte separation at a flow rate of 1 mL/min: gradient increase from 2% B to 70% B between 0−4 min, then immediate increase to 100% B until 4.5 min, and drop to 2% B after 4.5 min until the separation is finished at 5 min. The system was kept at 30 °C and DIBOA and DIBOA glycoside were monitored via a UV detector at 220 and 240 nm. Monitoring and data handling were operated using Chromeleon software (Thermofisher).

Glycosylation of niclosamide via GASP-predicted GT1s was carried out in reactions containing 50 μg/mL of each enzyme, 5 mM of UDP-Glc, and <1 mM niclosamide from a < 7 mM stock in 100% DMSO. Final niclosamide concentrations in the reactions are rough estimations since a significant amount of it could not be solubilized fully in DMSO even at 7 mM. Reactions with a total volume of 100 μL were run in a 50 mM potassium phosphate buffer (pH 7.45) with 50 mM NaCl at 30 °C and 300 rpm for 2 h. A hundred microliters of 100% methanol was added to terminate the reactions at the end of 2 h, followed by centrifugation at 2451g for 30 min at 4 °C to remove precipitations. Prior to HPLC analysis, 150 μL from the upper phase of each sample was added to an equal volume of methanol to facilitate niclosamide solubility further. The HPLC analysis was carried out as described for the DIBOA samples, except for a run time of 9 min and absorbance recording at 290 nm.

For niclosamide glycosylation via randomly selected GT1s, enzymes at varying concentrations were reacted with an undetermined amount of niclosamide and 3 mM UDP-Glc in a

https://doi.org/10.1021/acsomega.4c01583
ACS Omega 2024, 9, 27278−27288

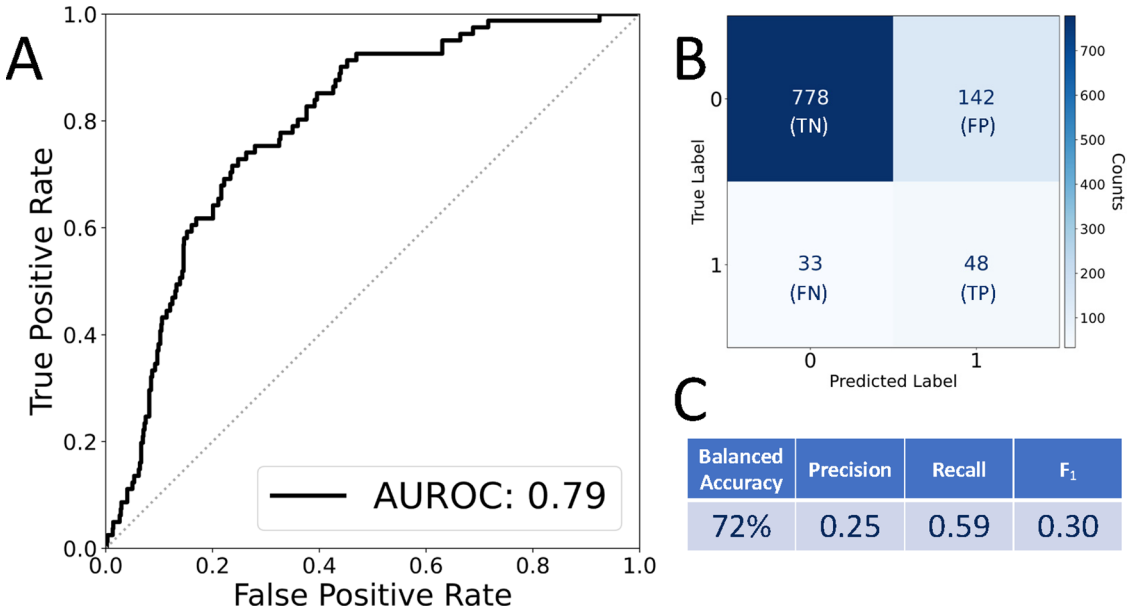

Figure 3. (A) ROC curve for GASP predictions on the in-house data set (black line) with the corresponding AUROC value. The gray dotted line corresponds to the random predictor. (B) Confusion matrix and (C) calculated test metrics of the GASP model on test data set using the probability threshold of 0.345 maximizing the F1 score.

buffer containing 50 mM HEPES and 50 mM NaCl (pH 7.0) overnight at 30 °C.

Chemical Feature Selection. To compare the importance of the 153 generated chemical substrate features, feature selection was performed. Individual features were deselected iteratively, where predictive performance was measured after temporarily leaving out each remaining feature. The feature whose removal led to the smallest decrease in performance was then left out permanently for further iterations until only one remained, which may be considered the most important single feature in discerning reactivity from nonreactivity. At each iteration, the available data points were randomly split into train and test sets, where the test set contained 20% of substrates. These were selected by randomly picking a single substrate and then finding its nearest neighbors based on the highest correlation on their chemical feature values. Performance metrics were averaged between 10 repetitions of each iteration.

The performance for each deselection was evaluated by a custom metric, named topP, which is designed to minimize false positives. This is motivated by predictor application, where experiments will only be carried out on the top-scoring predictions. Thus, this metric has a bias for the accuracy of top-scoring candidates rather than equal weight for all GT1:substrate pairs. TopP is defined by assigning weights from 1 to P to the top P predictions in ascending order, where P is the number of positives (reactive pairs). TopP is then equal to the sum of weights given to true positives, after normalization.

Moreover, as the MDS features are abstract values not representing a single chemical property, their use requires additional justification. Consequently, we studied their importance by training GASP models without any of the 12 MDS features and comparing the resulting performance to the full GASP model.

RESULTS

Test Data Set. For independent validation of predictor performance, a test data set was collected by measuring initial rates (k_{app}) of 24 GT1 enzymes from 15 different plants on 88 acceptors. This yielded a total of 1031 data points (not all acceptors were tested against all enzymes) of which 81 were active, 920 were inactive, and 30 were inconclusive. The inconclusive data points were removed from the data set yielding a total of 1001 data points with a distribution of 8% active and 92% inactive GT1:acceptor pairs (see "dataset1.xlsx" in the Supporting Information).

Algorithm Generation and Evaluation. The outputs of our enzyme and substrate feature generation pipelines are fed to a random forest classifier consisting of 1000 trees. We refer to this as the GASP model. It was trained on a curated published data set of 4160 data points, which were reactivity measurements between 77 chemicals and 73 GT1 enzymes (53 from *Arabidopsis thaliana*, 10 from *Lycium barbarum*, 6 from *Avena strigosa*, 2 from *Medicago truncatula*, 1 from *Streptomyces antibioticus*, and 1 from *Vitis vinifera*).[6] GASP was subsequently tested on the independent in-house test data set, with the predicted probabilities covering the full range of values (Figure S4). Here, the random forest predictor achieved an AUROC of 0.79 (where an AUROC of 0.5 indicates random guessing and a value of 1.0 indicates perfect classification) (Figure 3A). Interestingly, the performance does not appear to be determined solely by similarity to the training data, as observed when examining the performance from enzymes belonging to the same organisms (Figure S5). With a probability threshold of 0.345 corresponding to the maximum F_1-score of 0.30, a confusion matrix was calculated (Figure 3B) with a precision and recall of 0.25 and 0.59, respectively (Figure 3C). We observed a high number of false positives compared to true positives, probably due to the imbalance of labels in the test data, as the majority of the GT1:acceptor pairs are inactive (Figure 1). If the confusion matrix is normalized by the number of points in each class, we instead observe that only 15% of the inactive GT1:acceptor pairs are falsely predicted as reactive, while 85% are predicted correctly (Figure S6). A balanced accuracy of 72% was obtained, although it should be noted that by lowering the threshold to

https://doi.org/10.1021/acsomega.4c01583
ACS Omega 2024, 9, 27278−27288

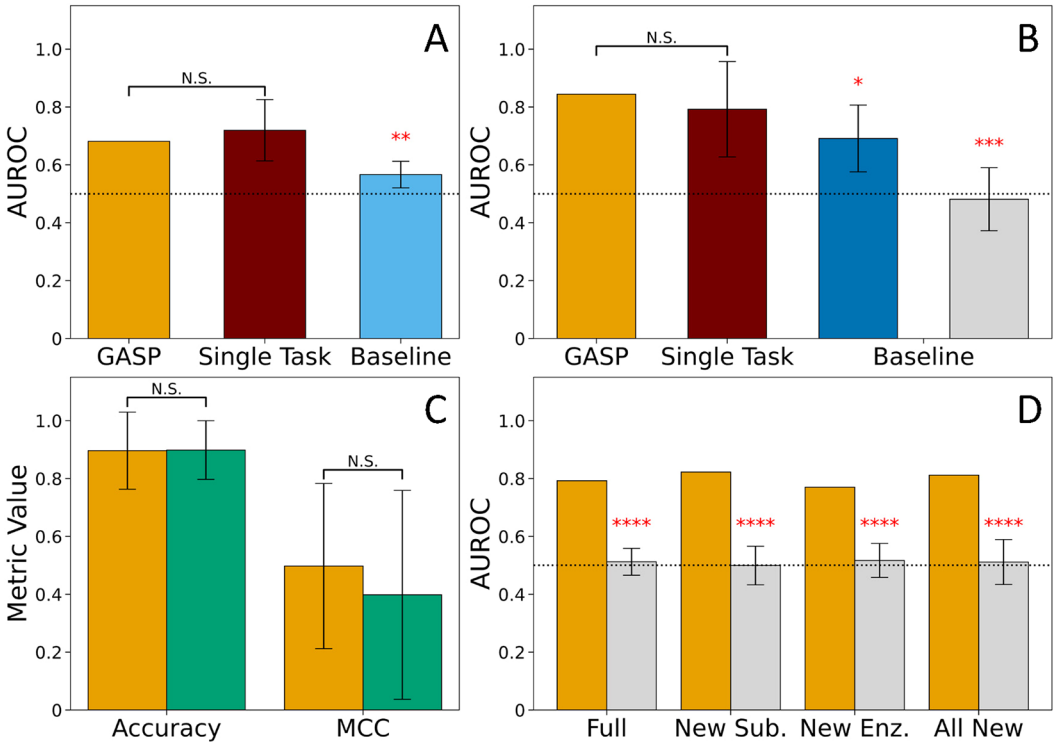

Figure 4. (A, B) Performance of the full GASP, single-task, and baseline models for both enzyme (A) and substrate (B) discovery (see Comparison to Baselines and Single-Task Models in Methods): Levenshtein KNN model (light blue), Tanimoto KNN model (dark blue), and Random features Ridge regression model (gray). Performance of single-task and baseline models was averaged over individual discovery models, with error bars denoting the standard deviation. All single-task and baseline models are compared to the performance of the full GASP model using a two-sided one-mean t test, with each additional asterisk representing significance at [0.05, 0.0005, 0.000001] thresholds, respectively, while N.S. denotes nonsignificant difference (p-value above 0.05). The dotted line corresponds to AUROC for the random predictor. (C) Comparison of performance of GASP (yellow) and GT-Predict (green) using the GT-Predict validation protocol. Average values are represented as bars, with the average accuracies calculated using 48 individual leave-one-out models and average MCC calculated using 32 individual models. Standard deviation is represented as error bars, with a two-sided t test resulting in a p-value of 0.918 between the accuracies and 0.227 for the MCC scores. Individual values are reported in Table S4. (D) Performance of GASP (yellow) and a baseline model (Random features Ridge regression model, gray) using different test sets consisting either of the full data set, GT1:acceptor pairs with the substrates not present in the training data, pairs with the enzymes not present, or pairs with both acceptor and enzyme being new to the model. Two-sided one-mean t tests between GASP the baseline model for all test subsets result in p-values essentially zero. The dotted line again corresponds to AUROC for the random predictor.

0.265, GASP can obtain the maximum balanced accuracy of 74% (Figure S7).

Comparison of GASP and Alternative Models. First, we validated the GASP architecture by following the protocol described by Goldman et al.,[18] constructing baseline and single-task models for both enzyme discovery and substrate discovery for the enzyme and substrate subsets with sufficient data (see Comparison to Baselines and Single-Task Models in Methods). We observed a significant increase in performance between the full GASP model and all baseline models (Figure 4A,B). Interestingly, the full model exhibited similar performance to the single-task GASP models within one standard deviation, indicating that the CPI nature of the full GASP model does not produce higher performance in the setting when sufficient experimental data for a given substrate or enzyme are available. This aligns with the conclusions by Goldman et al.[18] However, incorporating both enzyme and substrate features into the model did not compromise its performance and also enabled the full GASP model to predict new GT1:acceptor pairs without the need to collect sufficient training data and retrain a new single-task model. This is highlighted by the good model performance on both enzymes and substrates not present in the training data set, significantly outperforming the baseline model (Figure 4D).

We also compared GASP to the previously published GT-Predict model.[6] Due to the nature of the GT-Predict architecture, we were unable to use our in-house data set to test GT-Predict. Instead, we replicated their leave-one-out validation (see Comparison to GT-Predict in Methods). For both the average accuracy and average MCC score, the two models lie within one standard deviation of each other, and a two-sided t test reveal them to be statistically similar (Figure 4C, Table S4, p-value of 0.918 and 0.227 for the accuracies and MCC scores, respectively). This indicates that in the GT-predict setting, the models have equal performance. However, the pan-specificity unique to GASP allows it to automatically generate features and make predictions for new GT1:acceptor pairs (Figure 4D), which is a major practical benefit.

Correlation between GASP Predictions and Substrate Conversion Yields. There is a strong biotechnological interest in predicting which substrates a given enzyme could glycosylate with high synthetic yields. We recently published a data set evaluating the glycosylation yields of 32 structurally similar polyphenols,[28] which we further validated for the soybean GT1 enzyme *Gm*UGT88E3.[29] Clearly, GASP appeared to discriminate between the given 32 acceptors despite their high chemical similarity, assigning prediction scores ranging from 0.213 to 0.831 (Figure S8A). Interestingly,

https://doi.org/10.1021/acsomega.4c01583
ACS Omega 2024, 9, 27278−27288

Table 1. Ten Most Important Features Found from the Negative Feature Selection[a]

Order	1	2	3	4	5
Chemical feature	Fraction sp^3 carbons	MDS 9	No. of valence electrons	No. of saturated rings	No. of sulfide bonds
Order	**6**	**7**	**8**	**9**	**10**
Chemical feature	No. of furans	No. of Quaternary nitrogens	No. of aromatic nitrogens	NPR1	No. of aromatic rings

[a]NPR: normalized principal moment ratio, MDS: multidimensional scaling).

while there were a few false negatives (low prediction value, yet high synthetic yields), the top 2 predictions corresponded to quantitative yields, and the top 50% of predictions corresponded to reactions with >50% synthetic yields (Figure S8B). These results are definitely encouraging to explore the synthetic prospects of a given GT1 enzyme.

DIBOA Glycosylation by Expert-Selected versus Predicted GT1s. DIBOA is one of the most common benzoxazinoids in plants, taking part in plant defense. It is stored in the vacuole in its glycosylated form to reduce autotoxicity. Upon cell damage, a β-glucosidase hydrolyses the glycoside to release the toxic aglycon in response to pest or pathogen attack.[32] DIBOA is of interest as a phytoremediation agent due to its ability to degrade the recalcitrant herbicide atrazine,[33] and as a biopesticide due to its toxicity to pests and pathogens. There is only limited knowledge of GT1 enzymes active on DIBOA, and thus it is interesting to discover novel DIBOA-glycosylating enzymes.

BX8 and BX9 are two well-characterized GT1s that are known to glycosylate DIBOA,[30] thus were chosen as positive controls in this study. The DIBOA molecule carries two potential glycosylation sites, and our results indicate that while BX8 and BX9 each produce a single product, they present different regioselectivities as seen in two separate peaks with different retention times on HPLC spectra (Figure S9).

To discover novel DIBOA-glycosylating enzymes, we leveraged an in-house data set of 40 GT1s reactivity on different polyphenols.[28] On the basis of DIBOA's chemical similarity to some of the substrates in this data set (5,7-dihydroxychromone, 4,7-dihydroxycoumarin, 4-methylesculetin, and 4-methyllimetol), we selected six in-house GT1 enzymes to be assayed for DIBOA activity (referred to as "expert selection"). In parallel, we predicted DIBOA-active GT1 enzymes using GASP (Figure S10) and chose six of the top-ranking enzymes present in our stock (see Case Study: Glycosylation of GASP-Predicted GT1s vs Expert Selection and Random Selection in Methods). As summarized in Table S5, five out of six expert-selected GT1s showed activity on DIBOA, while for the GASP-predicted GT1s, the success rate was three out of six. Among expert-selected GT1s, only *Rh*Gt1 from *Rosa hybrid* was inactive. As for the remaining five, only GT171E5 from *Carthamus tinctorius* produced the same product as the BX9 enzyme, while the others showed the same product as BX8 (Figure S11). As the in-house data set does not provide any information about the regioselectivity of the reactive GT1:acceptor pairs, GASP is unable to predict this property. Nevertheless, a similar trend to the expert-selected GT1s was observed for the three active algorithm-predicted GT1s, namely GT184A57 from *Eutrema japonicum*, GT174F2 from *Arabidopsis thaliana*, and GT175L5 from *Lycium barbarum*, which all produced the same product as BX8 (Figure S12). It should be noted that the commercial DIBOA preparation used as a standard contained trace amounts of a compound with the same retention time as that produced by BX8, as can be seen in the HPLC spectra of the negative control samples. The corresponding peak area was subtracted.

Niclosamide Glycosylation by Random in-House versus Predicted GT1s. Niclosamide is a lipophilic and weakly acidic salicylanilide widely used as an antihelminth drug for the treatment of tapeworm infections.[34] Unfortunately, niclosamide's poor aqueous solubility reduces its bioavailability, which presents a major challenge for the realization of its pharmaceutical potential.[35] Glycosylation can be a powerful tool to increase the aqueous solubility of such compounds. Our previous random screening of in-house GT1 enzymes for niclosamide glycosylation had identified 10/19 (53%) active enzymes (Table S6), although the activities were very low, and conversion yields were too low to quantify. Hence, we employed GASP to predict efficient niclosamide-glycosylating GT1s (Figure S13). From the 12 sequences assessed, five could not be expressed in *E. coli*, and one was expressed in its insoluble form (Table S6). Five out of six remaining sequences, however, demonstrated significant niclosamide glycosylation activity as seen in the HPLC spectra (Figure S15). The GASP hit rate for the niclosamide case was thus 83% (5 out of 6).

Acceptor Features Important for Prediction Performance. To learn which of the 153 chemical features describing the acceptors were more important to prediction performance, we performed negative feature selection. The ten most important chemical features from the negative feature selection are shown in Table 1, where chemical features relating to atom hybridization and cyclic properties (i.e., number of saturated rings, aromatic rings, furan structures and aromatic nitrogens) are predominant. Indeed, the fraction of sp^3 hybridized carbons in a molecule is the most important feature, while also impacting the features ranked fourth, sixth, and tenth. The hybridization of nitrogen impacts features seventh and eighth. Since GT1s predominantly glycosylate polyphenolic compounds, and GASP was trained primarily on these compounds, it is compelling to observe that the performance depends on the description of cyclic structures.

It is worth noting that the negative feature selection ranks the chemical features based on their importance to achieve high accuracy, not whether these features favor glycosylation. Indeed, while the number of sulfide bonds (i.e., thioether) was ranked as the fifth most important feature, these were only present in three out of the 88 chemicals with none of them showing reactivity in 82 reactions.

To evaluate the usefulness of the MDS fingerprint reduction included in the chemical features, we evaluated the model's performance without its use: when removing all MDS values from the substrate feature set, we observed a decrease in

https://doi.org/10.1021/acsomega.4c01583
ACS Omega 2024, 9, 27278−27288

prediction performance (Figure S15). Together with a dimension of the MDS-generated space being the second most important feature, we conclude that the molecular fingerprints serve as relevant features for improving the model's performance, and the dimensionality reduction conserves useful information.

DISCUSSION

In this work, we demonstrated the synergistic effect of high-throughput data generation with a chemically informed machine learning predictor. Indeed, we proposed GASP, an enzyme specificity predictor trained on the largest experimental data set of GT1 enzymes which performs well on enzymes and acceptors absent from the training set. This was demonstrated using an independent test data set of 1001 data points, where GASP outperformed all baseline models. A leave-one-out comparison to the previous state-of-the-art model for predicting GT1:acceptor pairs, GT-Predict,[6] revealed a comparable accuracy but higher MCC score, demonstrating the potential of GASP. And while the full model also exhibited similar performance to single-task models, the pan-specificity of GASP allows it to readily incorporate and predict new GT1:acceptor pairs. This was observed when we examined the performance of GASP on GT1:acceptor pairs absent from the training data set, leading to only minimal changes in the AUROC. We also investigated the predictions for enzymes from individual organisms, where predictions on proteins from organisms absent from the training data showed good performance even when the phylogenetic similarity with *Arabidopsis thaliana*, which comprises the majority of the training data, was low. The model thereby exhibited the ability to accurately extrapolate beyond the training GT1:acceptor pairs, enabling researchers to estimate the substrate activity of new GT1 enzymes without requiring preliminary experimental analysis. It should be noted that the enzyme feature generation pipeline requires alignment of new sequences to the current consensus sequence, and sequences with very low similarity might result in a drop in performance.

To examine this application of GASP, we examined the correlation between the model probability output and the substrate conversion yields of a single GT1. We observed a positive correlation between the two properties, with the top predictions all having experimental yields. Importantly, GASP was solely trained on binary activity scores, while conversion yields are inherently quantitative. The ability of GASP to predict the changes in a separate property space is extremely promising, as it not only allows for a broader application of the model but also indicates that GASP is able to capture some of the intrinsic forces behind glycosyltransferases beyond binary activity.

We also conducted two use case studies with DIBOA and niclosamide. GASP outperformed a random selection of GT1s for the niclosamide case, as GASP had a hit rate of 83% compared to the 53% obtained with random selection. In the DIBOA case, a hit rate of 50% for the GASP-selected enzymes indicates that, not surprisingly, GASP cannot compete with highly trained researchers in the field, who got a hit rate of 83%. However, GASP can parse a much larger number of sequences, including never-assayed sequences, while expert selection is limited to sequences evaluated against analogues. In conclusion, these case studies show that GASP can be utilized as a tool for preliminary assessment of enzymes.

It should be noted that GASP is only trained to predict acceptor specificity. Due to the limitations of the training data, the model is incapable of estimating properties such as regioselectivity, bond formation, and donor specificity. Furthermore, GASP incorporates only the sequence of proteins. Nevertheless, it is interesting that GASP is successful despite the fact that the enzyme features are generated utilizing a multiple sequence alignment, and therefore, the algorithm does not directly use such important characteristics as loops of varying length near the active site, which are known to have a strong impact in CAZymes' specificity, including GT1s'.[36] With the recent release of AlphaFold2[37] and the wealth of accurate structural models it provides, it might be feasible to incorporate structural information of the overall protein fold as well as active site loops, similar to what has been done for the predictions of binding parameters of cellulases.[38] In addition to incorporating structural information, future models should address the issue of regioselectivity. While GASP only focused on predicting the acceptor specificity, partially due to the lack of the regiochemical outcome of GT1 glycosylation information in both our data sets and most of the literature, regioselectivity is an important property of the GT1 enzymes. ML models able to predict regioselectivity would thus be highly advantageous when selecting an appropriate GT1 for biocatalysis.

Finally, the developed pipelines enable the addition of new data, thus the present framework can be extended for generating new improved models on other data or in combination with the data used in this work. The provided pipelines for automated feature generation on proteins and chemicals can even be used for other enzyme classes. Furthermore, the in-house data set employed in this study offers a new, cleaned, and independent GT1 activity data set for use as training or test sets for future ML models.

ASSOCIATED CONTENT

Data Availability Statement

All activity data sets used herein are included in a supplemental zip file, and GASP code is available at https://github.com/degnbol/GASP.

Supporting Information

The Supporting Information is available free of charge at https://pubs.acs.org/doi/10.1021/acsomega.4c01583.

Additional experimental details, materials, methods, and results, including HPLC spectra, hyperparameter tuning, performance comparisons, and an appendix describing all acceptors (PDF)

GT1:acceptor reactivity data set used for testing the performance of GASP (XLSX)

AUTHOR INFORMATION

Corresponding Author

Ditte Hededam Welner − *DTU Biosustain, Technical University of Denmark, Lyngby, Denmark 2800;* orcid.org/0000-0001-9297-4133; Email: diwel@biosustain.dtu.dk

Authors

David Harding-Larsen − *DTU Biosustain, Technical University of Denmark, Lyngby, Denmark 2800*

Christian Degnbol Madsen − *DTU Biosustain, Technical University of Denmark, Lyngby, Denmark 2800; The*

https://doi.org/10.1021/acsomega.4c01583
ACS Omega 2024, 9, 27278−27288

University of Melbourne Faculty of Science, Melbourne Integrative Genomics, University of Melbourne, Melbourne, VIC 3052, Australia; orcid.org/0000-0001-8218-7160

David Teze − *DTU Biosustain, Technical University of Denmark, Lyngby, Denmark 2800;* orcid.org/0000-0002-6865-6108

Tiia Kittilä − *DTU Biosustain, Technical University of Denmark, Lyngby, Denmark 2800*

Mads Rosander Langhorn − *DTU Biosustain, Technical University of Denmark, Lyngby, Denmark 2800;* orcid.org/0009-0008-2156-6026

Hani Gharabli − *DTU Biosustain, Technical University of Denmark, Lyngby, Denmark 2800;* orcid.org/0000-0002-8195-2323

Mandy Hobusch − *DTU Biosustain, Technical University of Denmark, Lyngby, Denmark 2800*

Felipe Mejia Otalvaro − *DTU Biosustain, Technical University of Denmark, Lyngby, Denmark 2800*

Onur Kırtel − *DTU Biosustain, Technical University of Denmark, Lyngby, Denmark 2800*

Gonzalo Nahuel Bidart − *DTU Biosustain, Technical University of Denmark, Lyngby, Denmark 2800*

Stanislav Mazurenko − *Department of Experimental Biology and RECETOX, Faculty of Science, Masarykova Univerzita, Brno 625 00, Czech Republic; International Clinical Research Center, St. Anne's University Hospital Brno, Brno 656 91, Czech Republic*

Evelyn Travnik − *DTU Biosustain, Technical University of Denmark, Lyngby, Denmark 2800*

Complete contact information is available at: https://pubs.acs.org/10.1021/acsomega.4c01583

Author Contributions

D.H.-L. and C.D.M. contributed equally to this work.

Notes

The authors declare no competing financial interest.

■ ACKNOWLEDGMENTS

We thank The Novo Nordisk Foundation for supporting this work through Grants NNF18OC0034744, NNF10CC1016517, NNF20CC0035580, and NNF19SA0035438. This work was also supported by Czech Ministry of Education, Youth and Sports [ESFRI RECETOX RI LM2023069, ESFRI ELIXIR LM2023055] and the European Union's Horizon 2020 Research and Innovation Programme under Grant agreement no. 857560 (CETOCOEN Excellence). This publication reflects only the authors' views, and the European Commission is not responsible for any use that may be made of the information it contains. The authors thank Tiia Kittilä and Folmer Fredslund for selecting sequences for the in-house dataset and Valeria Della Gala for preliminary work on DIBOA. Figures [1] and [2] were created with BioRender.com.

■ REFERENCES

(1) Nidetzky, B.; Gutmann, A.; Zhong, C. Leloir Glycosyltransferases as Biocatalysts for Chemical Production. *ACS Catal.* **2018**, *8* (7), 6283−6300.

(2) De Roode, B. M.; Franssen, M. C. R.; Van Der Padt, A.; Boom, R. M. Perspectives for the Industrial Enzymatic Production of Glycosides. *Biotechnol. Prog.* **2003**, *19* (5), 1391−1402.

(3) Desmet, T.; Soetaert, W.; Bojarova, P.; Kren, V.; Dijkhuizen, L.; Eastwick-Field, V.; Schiller, A. Enzymatic Glycosylation of Small Molecules: Challenging Substrates Require Tailored Catalysts. *Chem.—Eur. J.* **2012**, *18* (35), 10786−10801.

(4) Bowles, D.; Isayenkova, J.; Lim, E. K.; Poppenberger, B. Glycosyltransferases: Managers of Small Molecules. *Curr. Opin Plant Biol.* **2005**, *8* (3), 254−263.

(5) Lim, E. K.; Ashford, D. A.; Hou, B.; Jackson, R. G.; Bowles, D. J. Arabidopsis Glycosyltransferases as Biocatalysts in Fermentation for Regioselective Synthesis of Diverse Quercetin Glucosides. *Biotechnol. Bioeng.* **2004**, *87* (5), 623−631.

(6) Yang, M.; Fehl, C.; Lees, K. V.; Lim, E. K.; Offen, W. A.; Davies, G. J.; Bowles, D. J.; Davidson, M. G.; Roberts, S. J.; Davis, B. G. Functional and Informatics Analysis Enables Glycosyltransferase Activity Prediction. *Nat. Chem. Biol.* **2018**, *14* (12), 1109−1117.

(7) Drula, E.; Garron, M. L.; Dogan, S.; Lombard, V.; Henrissat, B.; Terrapon, N. The Carbohydrate-Active Enzyme Database: Functions and Literature. *Nucleic Acids Res.* **2022**, *50* (D1), D571−D577.

(8) Bidart, G. N.; Putkaradze, N.; Fredslund, F.; Kjeldsen, C.; Ruiz, A. G.; Duus, J. Ø.; Teze, D.; Welner, D. H. Family 1 Glycosyltransferase UGT706F8 from *Zea Mays* Selectively Catalyzes the Synthesis of Silibinin 7-O-β-D-Glucoside. *ACS Sustain Chem. Eng.* **2022**, *10*, 5078.

(9) Ross, J.; Li, Y.; Lim, E.-K.; Bowles, D. J. Higher Plant Glycosyltransferases. *Genome Biol.* **2001**, *2* (2), 3004.1−3004.6.

(10) Tegl, G.; Nidetzky, B. Leloir Glycosyltransferases of Natural Product C-Glycosylation: Structure, Mechanism and Specificity. *Biochem. Soc. Trans.* **2020**, *48* (4), 1583−1598.

(11) Lairson, L. L.; Henrissat, B.; Davies, G. J.; Withers, S. G. Glycosyltransferases: Structures, Functions, and Mechanisms. *Annu. Rev. Biochem.* **2008**, *77*, 521−555.

(12) Teze, D.; Coines, J.; Fredslund, F.; Dubey, K. D.; Bidart, G. N.; Adams, P. D.; Dueber, J. E.; Svensson, B.; Rovira, C.; Welner, D. H. *O*-/*N*-/*S*-Specificity in Glycosyltransferase Catalysis: From Mechanistic Understanding to Engineering. *ACS Catal.* **2021**, *11* (11), 1810−1815.

(13) He, J.-B.; Zhao, P.; Hu, Z.-M.; Liu, S.; Kuang, Y.; Zhang, M.; Li, B.; Yun, C.-H.; Qiao, X.; Ye, M. Molecular and Structural Characterization of a Promiscuous *C*-Glycosyltransferase from *Trollius Chinensis*. *Angew. Chem., Int. Ed.* **2019**, *131* (131), 11637−11644.

(14) Zhang, L.; Wang, D.; Zhang, P.; Wu, C.; Li, Y. Promiscuity Characteristics of Versatile Plant Glycosyltransferases for Natural Product Glycodiversification. *ACS Synth. Biol.* **2022**, *11* (11), 812−819.

(15) Ross, J.; Li, Y.; Lim, E.-K.; Bowles, D. J. Higher Plant Glycosyltransferases. *Genome Biology 2001 2:2* **2001**, *2* (2), 1−6.

(16) Yang, K. K.; Wu, Z.; Arnold, F. H. Machine-Learning-Guided Directed Evolution for Protein Engineering. *Nat. Methods* **2019**, *16* (8), 687−694.

(17) Mazurenko, S.; Prokop, Z.; Damborsky, J. Machine Learning in Enzyme Engineering. *ACS Catal.* **2020**, *10* (10), 1210−1223.

(18) Goldman, S.; Das, R.; Yang, K. K.; Coley, C. W. Machine Learning Modeling of Family Wide Enzyme-Substrate Specificity Screens. *PloS Comput. Biol.* **2022**, *18* (2), No. e1009853.

(19) Robinson, S. L.; Smith, M. D.; Richman, J. E.; Aukema, K. G.; Wackett, L. P. Machine Learning-Based Prediction of Activity and Substrate Specificity for OleA Enzymes in the Thiolase Superfamily. *Synth Biol.* **2020**, *5* (1), 1 DOI: 10.1093/synbio/ysaa004.

(20) Taujale, R.; Venkat, A.; Huang, L. C.; Zhou, Z.; Yeung, W.; Rasheed, K. M.; Li, S.; Edison, A. S.; Moremen, K. W.; Kannan, N. *Elife* **2020**, *9*, 1 DOI: 10.7554/eLife.54532.

(21) Robinson, S. L.; Terlouw, B. R.; Smith, M. D.; Pidot, S. J.; Stinear, T. P.; Medema, M. H.; Wackett, L. P. Global Analysis of Adenylate-Forming Enzymes Reveals β-Lactone Biosynthesis Pathway in Pathogenic Nocardia. *J. Biol. Chem.* **2020**, *295* (44), 14826−14839.

(22) Feehan, R.; Montezano, D.; Slusky, J. S. G. Machine Learning for Enzyme Engineering, Selection and Design. *Protein Eng Des Sel.* **2021**, *34*, 1−10.

(23) Edgar, R. C. MUSCLE: Multiple Sequence Alignment with High Accuracy and High Throughput. *Nucleic Acids Res.* **2004**, *32* (5), 1792−1797.

(24) Szöcs, E.; Stirling, T.; Scott, E. R.; Scharmüller, A.; Schäfer, R. B. Webchem: An R Package to Retrieve Chemical Information from the Web. *J. Stat Softw* **2020**, *93*, 1−17.
(25) Axen, S. D.; Huang, X. P.; Cáceres, E. L.; Gendelev, L.; Roth, B. L.; Keiser, M. J. A Simple Representation of Three-Dimensional Molecular Structure. *J. Med. Chem.* **2017**, *60* (17), 7393−7409.
(26) Chen, C. R.; Makhatadze, G. I. ProteinVolume: Calculating Molecular van Der Waals and Void Volumes in Proteins. *BMC Bioinformatics* **2015**, *16* (1), 1−6.
(27) Pedregosa, F.; Michel, V.; Grisel, O.; Blondel, M.; Prettenhofer, P.; Weiss, R.; Vanderplas, J.; Cournapeau, D.; Pedregosa, F.; Varoquaux, G.; Gramfort, A.; Thirion, B.; Grisel, O.; Dubourg, V.; Passos, A.; Brucher, M.; Perrot, M.; Duchesnay, C9. Scikit-Learn: Machine Learning in Python. *Journal of Machine Learning Research* **2011**, *12* (85), 2825−2830.
(28) de Boer, R. M.; Vaitkus, D.; Enemark-Rasmussen, K.; Maschmann, S.; Teze, D.; Welner, D. H. Regioselective Glycosylation of Polyphenols by Family 1 Glycosyltransferases: Experiments and Simulations. *ACS Omega* **2023**, *8* (48), 46300−46308.
(29) de Boer, R. M.; Hvid, D. E. H.; Davail, E.; Vaitkus, D.; Duus, J. Ø.; Welner, D. H.; Teze, D. Promiscuous Yet Specific: A Methionine-Aromatic Interaction Drives the Reaction Scope of the Family 1 Glycosyltransferase GmUGT88E3 from Soybean. *Biochemistry* **2023**, *62* (23), 3343−3346.
(30) Von Rad, U.; Hüttl, R.; Lottspeich, F.; Gierl, A.; Frey, M. Two Glucosyltransferases Are Involved in Detoxification of Benzoxazinoids in Maize. *Plant Journal* **2001**, *28* (6), 633−642.
(31) Hon, J.; Marusiak, M.; Martinek, T.; Kunka, A.; Zendulka, J.; Bednar, D.; Damborsky, J. SoluProt: prediction of soluble protein expression in Escherichia coli. *Bioinformatics* **2021**, *37* (1), 23−28.
(32) Frey, M.; Schullehner, K.; Dick, R.; Fiesselmann, A.; Gierl, A. Benzoxazinoid Biosynthesis, a Model for Evolution of Secondary Metabolic Pathways in Plants. *Phytochemistry* **2009**, *70* (15−16), 1645−1651.
(33) Willett, C. D.; Lerch, R. N.; Lin, C. H.; Goyne, K. W.; Leigh, N. D.; Roberts, C. A. Benzoxazinone-Mediated Triazine Degradation: A Proposed Reaction Mechanism. *J. Agric. Food Chem.* **2016**, *64* (24), 4858−4865.
(34) Pearson, R. D.; Hewlett, E. L. Niclosamide Therapy for Tapeworm Infections. *Ann. Int. Med.* **1985**, *102* (4), 550.
(35) Needham, D. The PH Dependence of Niclosamide Solubility, Dissolution, and Morphology: Motivation for Potentially Universal Mucin-Penetrating Nasal and Throat Sprays for COVID19, Its Variants and Other Viral Infections. *Pharm. Res.* **2022**, *39* (1), 115−141.
(36) Brazier-Hicks, M.; Offen, W. A.; Gershater, M. C.; Revett, T. J.; Lim, E. K.; Bowles, D. J.; Davies, G. J.; Edwards, R. Characterization and Engineering of the Bifunctional N- and O-Glucosyltransferase Involved in Xenobiotic Metabolism in Plants. *Proc. Natl. Acad. Sci. U. S. A.* **2007**, *104* (51), 20238−20243.
(37) Jumper, J.; Evans, R.; Pritzel, A.; Green, T.; Figurnov, M.; Ronneberger, O.; Tunyasuvunakool, K.; Bates, R.; Žídek, A.; Potapenko, A.; Bridgland, A.; Meyer, C.; Kohl, S. A. A.; Ballard, A. J.; Cowie, A.; Romera-Paredes, B.; Nikolov, S.; Jain, R.; Adler, J.; Back, T.; Petersen, S.; Reiman, D.; Clancy, E.; Zielinski, M.; Steinegger, M.; Pacholska, M.; Berghammer, T.; Bodenstein, S.; Silver, D.; Vinyals, O.; Senior, A. W.; Kavukcuoglu, K.; Kohli, P.; Hassabis, D. Highly Accurate Protein Structure Prediction with AlphaFold. *Nature* **2021**, *596* (7873), 583−589.
(38) Schaller, K. S.; Kari, J.; Borch, K.; Peters, H. J.; Westh, P. Binding Prediction of Multi-Domain Cellulases with a Dual-CNN. *arXiv*; 02698v1 [physics. bio-ph], **2022**, DOI: 10.48550/arXiv.2207.02698.

https://doi.org/10.1021/acsomega.4c01583
ACS Omega 2024, 9, 27278−27288